

Credentialing a Preclinical Mouse Model of Alveolar Rhabdomyosarcoma

Koichi Nishijo,¹ Qing-Rong Chen,^{5,6} Lei Zhang,⁷ Amanda T. McCleish,¹ Andrea Rodriguez,¹ Min Jung Cho,¹ Suresh I. Prajapati,¹ Jonathan A.L. Gelfond,² Gary B. Chisholm,² Joel E. Michalek,² Bruce J. Aronow,⁸ Frederic G. Barr,⁹ R. Lor Randall,¹⁰ Marc Ladanyi,¹¹ Stephen J. Qualman,¹³ Brian P. Rubin,¹² Robin D. LeGallo,¹³ Chiayeng Wang,⁷ Javed Khan,⁵ and Charles Keller^{1,3,4}

¹Greehey Children's Cancer Research Institute and Departments of ²Epidemiology and Biostatistics, ³Pediatrics, and ⁴Cellular and Structural Biology, University of Texas Health Science Center, San Antonio, Texas; ⁵Oncogenomics Section, Pediatric Oncology Branch, National Cancer Institute, Gaithersburg, Maryland; ⁶Advanced Biomedical Computing Center, Science Applications International Corporation-Frederick, Inc., Frederick, Maryland; ⁷Center for Molecular Biology of Oral Diseases, University of Illinois at Chicago, Chicago, Illinois; ⁸University of Cincinnati College of Medicine, Cincinnati, Ohio; ⁹Department of Pathology and Laboratory Medicine, University of Pennsylvania School of Medicine, Philadelphia, Pennsylvania; ¹⁰Department of Orthopedics, University of Utah, Salt Lake City, Utah; ¹¹Department of Pathology and Human Oncology and Pathogenesis Program, Memorial Sloan-Kettering Cancer Center, New York, New York; ¹²Department of Anatomic Pathology, Cleveland Clinic, Cleveland, Ohio; and ¹³Children's Research Institute, Columbus Children's Hospital, Columbus, Ohio

Abstract

The highly aggressive muscle cancer alveolar rhabdomyosarcoma (ARMS) is one of the most common soft tissue sarcoma of childhood, yet the outcome for the unresectable and metastatic disease is dismal and unchanged for nearly three decades. To better understand the pathogenesis of this disease and to facilitate novel preclinical approaches, we previously developed a conditional mouse model of ARMS by faithfully recapitulating the genetic mutations observed in the human disease, i.e., activation of *Pax3:Fkhr* fusion gene with either *p53* or *Cdkn2a* inactivation. In this report, we show that this model recapitulates the immunohistochemical profile and the rapid progression of the human disease. We show that *Pax3:Fkhr* expression increases during late preneoplasia but tumor cells undergoing metastasis are under apparent selection for *Pax3:Fkhr* expression. At a whole-genome level, a cross-species gene set enrichment analysis and metagene projection study showed that our mouse model is most similar to human ARMS when compared with other pediatric cancers. We have defined an expression profile conserved between mouse and human ARMS, as well as a *Pax3:Fkhr* signature, including the target gene, *SKP2*. We further identified 7 "druggable" kinases overexpressed across species. The data affirm the accuracy of this genetically engineered mouse model. [Cancer Res 2009;69(7):2902–11]

Introduction

Rhabdomyosarcoma is the most common soft tissue tumor in childhood (1). Pediatric rhabdomyosarcoma can be divided into two major subtypes, embryonal rhabdomyosarcoma (ERMS) and alveolar rhabdomyosarcoma (ARMS; ref. 1). ERMS comprises 50% to 60% of all rhabdomyosarcoma cases and typically manifests a favorable outcome, whereas 20% to 30% of rhabdomyosarcoma are of the more aggressive alveolar subtype that is associated with frequent metastasis at the time of initial diagnosis (2). The

development of more effective therapies in ARMS, however, has been hampered by a lack of knowledge about basic molecular mechanisms of tumor development. Cytogenetic and molecular studies show that 70% to 85% of ARMS have balanced chromosomal translocations of t(2;13) or t(1;13), which lead to the formation of chimeric transcription factors consisting of the NH₂ terminal regions of *Pax3* or *Pax7* fused to the COOH terminal region of *Fkhr* (3). *Pax3:Fkhr*-positive ARMS is more aggressive than *Pax7:Fkhr*-positive or fusion-negative ARMS; thus, *Pax3:Fkhr*-positive ARMS represents the most clinically intractable subset of ARMS (4).

We previously generated a conditional knock-in allele of *Pax3:Fkhr* in *Pax3* locus and established a mouse model of ARMS by simultaneously activating *Pax3:Fkhr* expression and inactivating *p53* or *Cdkn2a* in *Myf6*-expressing maturing myofibers (5–7). In the current study, we show that this model authentically recapitulates the natural history, histologic features, and genetic features of the human disease, and we show the utility of this model in understanding the aspects of disease progression and therapeutic target identification.

Materials and Methods

Mice. The conditional models of ARMS have been previously described (5). At necropsy, animals were sacrificed by CO₂ asphyxiation in accordance with an approved Institutional Animal Care and Use Committee protocol. Characteristics of mouse tumor and skeletal muscle samples used for microarray and quantitative reverse transcription-PCR (qRT-PCR) are described in Supplementary Tables S1 and S2.

Real-time RT-PCR. qRT-PCR analyses were performed by a Taqman assay for mouse *Pax3:Fkhr* expression or by SYBR Green assay (PE Applied Biosystems) for other genes of interest. Primer and probe sequences are shown in Supplementary Tables S3 and S4.

Gene expression analysis. Gene expression analysis was performed using Affymetrix Mouse 430A arrays (Affymetrix). Original CEL files of the mouse ARMS are uploaded in the Gene Expression Omnibus site.¹⁴ For human tumors, published data sets of rhabdomyosarcomas (8, 9), juvenile and old skeletal muscles (10), Duchene muscular dystrophy (11), and a series of mesenchymal tumors (12, 13) and pediatric malignancies (14) were used (Supplementary Table S5). For mouse tumors, published data sets of

Note: Supplementary data for this article are available at Cancer Research Online (<http://cancerres.aacrjournals.org/>).

Requests for reprints: Charles Keller, 8403 Floyd Curl Drive MC7784, San Antonio, TX 78229-3900. Phone: 210-562-9062; Fax: 210-562-9014; E-mail: kellerc2@uthscsa.edu.

©2009 American Association for Cancer Research.

doi:10.1158/0008-5472.CAN-08-3723

¹⁴ <http://www.ncbi.nlm.nih.gov/geo/>

osteosarcoma (15) and medulloblastoma (16) were used. Methods of microarray analysis, including gene set enrichment analysis (GSEA) and metagene analysis, are described in Supplementary Materials and Methods.

CAT and luciferase reporter assays. CAT constructs containing *SKP2* promoter were described previously (17). The 220-bp genomic fragment 49-kb 3' to *Skp2* gene was inserted into pGL4.24 vector (Promega). Reporter plasmids were cotransfected with *Pax3:Fkhr* and *p53* into NIH3T3 cells or *p53*-deficient mouse embryonic fibroblasts (MEF).

Western blotting. Western blotting was performed as previously described (18). Antibodies against p27Kip1 (C-19), Skp2 (H-435), and Fkhr (C-20) were from Santa Cruz. Pax3 antibody (ab-2) was from Geneka. α -Tubulin antibody was from Oncogene.

Results

Biallelic activation of *Pax3:Fkhr* and disruption of *p53* or *Cdkn2a* are necessary for high penetrance of ARMS. The mean latency of ARMS development was 110 days with 100% penetrance of ARMS when biallelic activation of conditional *Pax3:Fkhr* allele was combined with homozygous deletion of conditional *p53* allele (Fig. 1A). However, when the mice had homozygous *Pax3:Fkhr* and heterozygous *p53* mutant alleles or heterozygous *Pax3:Fkhr* and homozygous *p53* mutant allele combinations, tumor incidence was significantly lower than that of double homozygous alleles ($P < 0.001$), indicating a mutation dosage effect. As previously described, activation of *Pax3:Fkhr* was necessary but not sufficient for ARMS development (5). When *Pax3:Fkhr* allele was combined with conditional *Cdkn2a* mutation, mice still required biallelic activation of both mutations to develop ARMS at 100% penetrance (Fig. 1B). There was no significant difference in ARMS development between *Pax3:Fkhr-p53* mice and *Pax3:Fkhr-Cdkn2a* mice (Fig. 1C). All ARMS cases were diagnosed by a qualified pathologist based upon histology, as well as MyoD and Myogenin immunohistochemistry (Fig. 1D). To determine the relative contribution of *p53* mutation to the development of ARMS, *Myf6^{ICNm/WT}Pax3^{P3Fm/P3Fm}p53^{F2-10/F2-10}* tumors were compared with *Myf6^{ICNm/WT}Pax3^{WT/WT}p53^{F2-10/F2-10}* tumors (Supplementary Fig. S1). *Myf6^{ICNm/WT}Pax3^{WT/WT}p53^{F2-10/F2-10}* tumors developed pleomorphic rhabdomyosarcomas at a much lower frequency than the ARMS seen in *Myf6^{ICNm/WT}Pax3^{P3Fm/P3Fm}p53^{F2-10/F2-10}* mice ($P < 0.001$, log-rank test). These findings suggest that the tumors from *Myf6^{ICNm/WT}Pax3^{P3Fm/P3Fm}p53^{F2-10/F2-10}* mice are not caused solely by *p53* mutation but by cooperating effects of *Pax3:Fkhr* and *p53* mutation.

Conditional mouse models of ARMS share the aggressive features of the human disease. The sites of tumors and stages at necropsy are summarized in Supplementary Tables 7A and 7B. Both *Pax3:Fkhr*, *p53* and *Pax3:Fkhr*, *Cdkn2a* models developed advanced ARMS tumors, although the frequency of distant hematogenous metastasis in *Pax3:Fkhr*, *p53* model was significantly higher than in *Pax3:Fkhr*, *Cdkn2a* model (χ^2 test, $P < 0.0001$). These conditional mouse models showed a predisposition to rapid disease progression, including rapid local tumor growth and invasion, regional lymph node involvement, and distant hematogenous metastasis (Fig. 2A–D; Supplementary Table S7B). For the latter, micro-CT scan showed both macrometastases and alveolar macrophages associated with micrometastases (Fig. 2C and D).

Transcriptional activation of *Pax3:Fkhr* is associated with ARMS progression. Although expression of *Pax3:Fkhr* fusion gene is driven by *Pax3* promoter in both human ARMS and in our conditional mouse models, promoter activity of *Pax3* is predicted to be low in mature myofibers (19). To monitor expression level of

Pax3:Fkhr during disease progression, we performed qRT-PCR of *Pax3:Fkhr* in adult skeletal muscles from wild-type (WT) and *Myf6^{ICNm/WT}Pax3^{P3Fm/P3Fm}p53^{F2-10/F2-10}* mice, as well as primary and metastatic ARMS tumors from *Myf6^{ICNm/WT}Pax3^{P3Fm/P3Fm}p53^{F2-10/F2-10}* mice (Fig. 3A). Samples are detailed in Supplementary Table S2. As expected, expression of *Pax3:Fkhr* in *Myf6^{ICNm/WT}Pax3^{P3Fm/P3Fm}p53^{F2-10/F2-10}* preneoplastic skeletal muscle was low, whereas *Pax3:Fkhr* expression was >100-fold higher in ARMS tumors. Metastatic tumors expressed *Pax3:Fkhr* at incrementally higher levels than the primary tumors. *Pax3:Fkhr* in the mouse tumor tissues were also detected at protein level using anti-Fkhr antibody (Fig. 3B). We also performed immunofluorescent analysis of corresponding tissue samples using anti-GFP antibody as an *in situ* correlate of *Pax3:Fkhr* expression (Fig. 3C). In our mice, *Pax3:Fkhr* is followed by an internal ribosomal entry site and the *eYFP* gene; therefore, *eYFP* expression corresponds to transcriptional activation of *Pax3:Fkhr* in these tissues (5). Whereas *eYFP* was undetectable in WT and preneoplastic adolescent skeletal muscle, primary and metastatic ARMS tumors strongly expressed *eYFP*. Expression pattern of *eYFP* in primary tumors was heterogeneous compared with the uniform expression pattern in metastatic tumors; quantitatively, the number of *eYFP*-expressing cells in metastatic ARMS tumors was higher than primary tumors (90% versus 33%, $P < 0.001$). These results suggest that the level of the transcriptional activation of *Pax3:Fkhr* is linked to tumor development and progression and that cooperative cellular events are required in the transformation from preneoplasia to tumor to activate *Pax3:Fkhr* transcription. Later, higher quantitative *Pax3:Fkhr* levels by RT-PCR for metastatic tumor lesions seems to be attributable to the more uniform expression of *Pax3:Fkhr* in tumor cells, but not necessarily higher expression in any individual cell.

Cross-species comparison of molecular signatures validates the mouse model as representative of human ARMS. GSEA is a computational method, which has been successfully used to assess whether pathways are conserved between zebrafish and human rhabdomyosarcoma (20, 21). For our GSEA, we tested whether the gene sets up-regulated in mouse ARMS are enriched in human ARMS when compared with other mesenchymal malignancies. The differentially expressed genes were selected by comparing mouse ARMS to 4-week-old WT skeletal muscle at P value of <0.01. Using published database of human sarcomas (13), we performed GSEA with up-regulated gene sets of mouse ARMS (list in Supplementary Table S8). The gene set up-regulated in mouse ARMS was enriched most significantly in human ARMS among all human mesenchymal malignancies (normalized enrichment score = 2.0720, FDR q val < 0.001; Supplementary Table S9). ERMS scored lower (normalized enrichment score = 1.5773, FDR q val = 0.0038). Additional GSEA results using a human rhabdomyosarcoma data set (9) are given in Supplementary Fig. S2.

Tamayo and colleagues recently developed a metagene projection methodology to enable a direct cross-species and cross-platform comparison (22). This method can be used to assess the degree to which mouse ARMS displays a transcriptional profile comparable with other human tumors (15). For the purpose of further investigating whether mouse ARMS shares genetic features of human ARMS, metagene projection analysis was undertaken. To define a metagene for human ARMS compared with other human tumors, we used previously published data sets of human mesenchymal tumors (13) and pediatric tumors (14). Although a metagene was defined for each human malignancy, projected

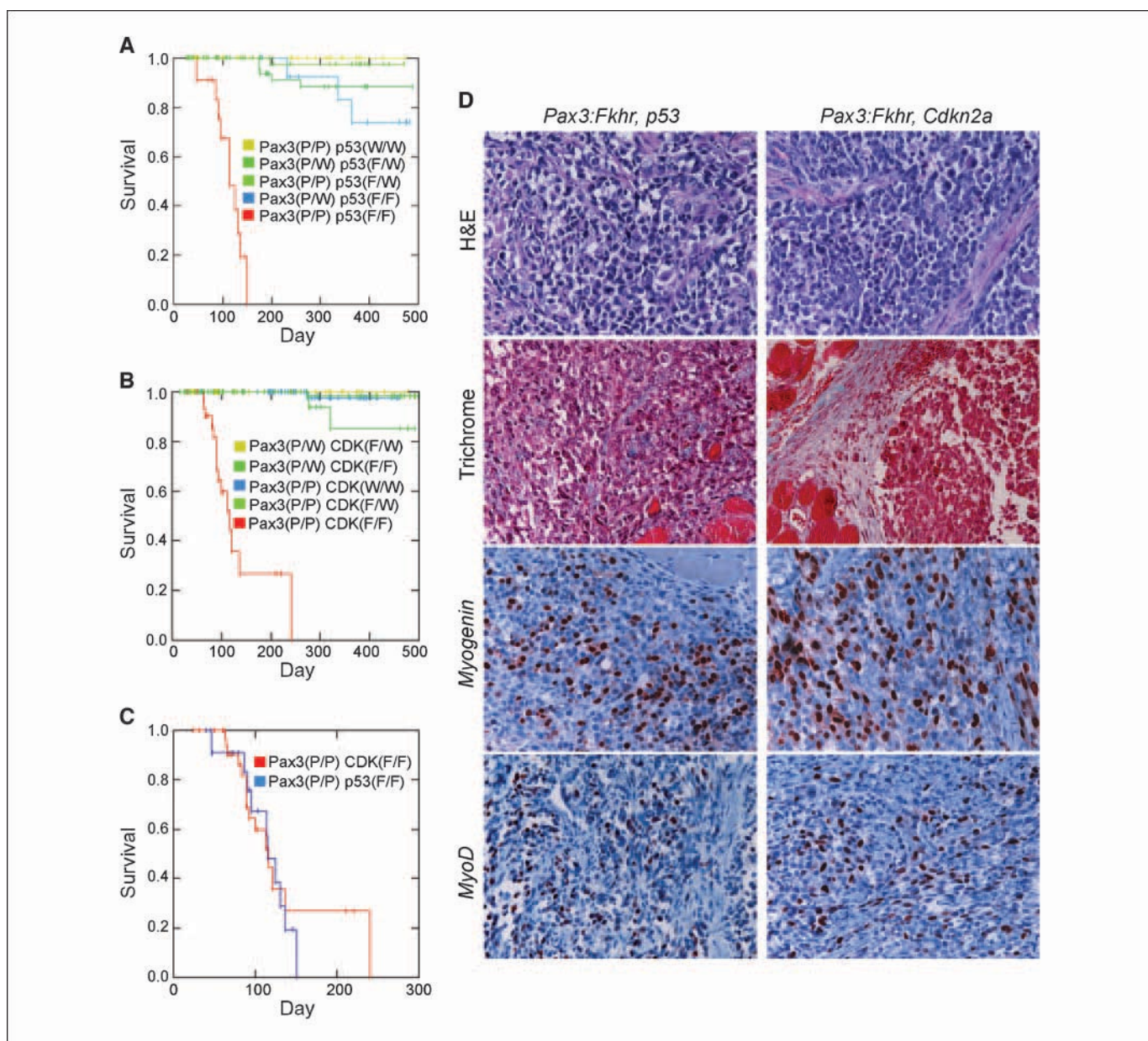


Figure 1. High penetrance of conditional mouse model of ARMS. Biallelic activation of *Pax3:Fkhr* expression concurrent with *p53* or *Cdkn2a* inactivation is critical for ARMS development. Disease-free survival of *Pax3:Fkhr, p53* mice (A) and *Pax3:Fkhr, Cdkn2a* mice (B). P, conditional *Pax3:Fkhr* allele; F, floxed conditional knockout allele; WT, WT allele. C, comparison of *Myf6^{CNm/WT}Pax3^{P3Fm/P3Fm}p53^{F2-10/F2-10}* [*Pax3(P/P) p53(F/F)*] and *Myf6^{CNm/WT}Pax3^{P3Fm/P3Fm}Cdkn2a^{F2-3/F2-3}* mice [*Pax3(P/P) CDK(F/F)*]. For cohort size, see Supplementary Table S6. D, H&E staining (top), trichrome staining (second row), immunohistochemistry positive for Myogenin (third row), and MyoD (bottom) in *Pax3:Fkhr, p53*, and *Pax3:Fkhr, Cdkn2a* mouse tumors.

clustering could not entirely separate human ARMS and ERMS (Supplementary Fig. S3A). In addition to our six cases of mouse ARMS samples, published mouse osteosarcoma samples (15) and mouse medulloblastoma samples (16) were used as testing samples. The projected clustering of mouse tumors showed mouse ARMS cluster with human rhabdomyosarcomas (both ARMS and ERMS) and mouse osteosarcomas and medulloblastomas cluster with their human counterparts. Another metagene analysis was performed using a well-characterized data set of human rhabdomyosarcoma (9). Again, however, a defined metagene failed to separate human ARMS and human ERMS completely; instead, 7 of 22 human ARMS clustered with human ERMS (Supplementary

Fig. S3B). Hierarchical clustering after metagene projection showed that mouse ARMS cluster with those seven cases of human ARMS, which confirmed that mouse ARMS recapitulates, at least, a subset of human ARMS cases.

The previous literature (8, 9, 23) has identified a subset of genes, which are specifically overexpressed in human ARMS compared with ERMS. Lae and colleagues (9) compared those gene sets and identified 11 genes that are shared in all of those three publications. To further validate that the mouse tumors share the genetic features of human ARMS, expression of those 11 genes, as well as *Mycn*, another representative alveolar specific gene, were examined by qRT-PCR (Fig. 4) among those 12 genes,

nine genes (*Ass1*, *Cnr1*, *Dcx*, *Ela1*, *Foxf1a*, *Pipox*, *Tcfap2b*, *Wscd1*, and *Mycn*) were significantly overexpressed compared with skeletal muscle. Thus, collectively, mouse ARMS tumors share a common core expression profile with human ARMS tumors.

Cross-species comparison of mouse and human Pax3:Fkhr-positive ARMS identifies a conserved expression signature of ARMS and permits Pax3:Fkhr target identification. To identify a conserved molecular profile of ARMS across species, genes differentially expressed in mouse tumors compared with WT skeletal muscle were projected into human rhabdomyosarcoma versus skeletal muscle. For the human data, published data sets of human young, old, and pathologic skeletal muscle (10, 11) and human rhabdomyosarcoma (8) were used. Genes (1,624) were differentially expressed in mouse ARMS versus skeletal muscle (673 up-regulated genes and 951 down-regulated genes in mouse ARMS; Supplementary Table S8). Among those 1,624 genes, 1,046 genes (392 of 673 up-regulated genes and 654 of 951 down-regulated genes) were also differentially expressed in human ARMS ($P < 0.01$ by *t* test in tumors of both species compared with skeletal

muscle; Supplementary Fig. S4A). This list may be a mixture of tumor-related and non-tumor-related genes, especially knowing that *in vivo* studies have shown that Pax3:Fkhr can not only cause tumors but also lead to abnormally developed, disordered (dystrophic) muscle (7, 24). Therefore, we sought to enrich for tumor-specific genes by excluding genes differentially expressed by diseased muscle, thus highlighting 368 genes in the cross-species molecular profile of ARMS (158 up-regulated and 210 down-regulated genes; Supplementary Table S8).

Using a different approach, we went on to identify a Pax3:Fkhr molecular signature conserved across species by combining the 1,624 mouse genes differentially expressed between mouse ARMS with the set of human Pax3:Fkhr-positive ARMS versus fusion-negative ARMS ($P < 0.01$; Supplementary Fig. S3B; gene list in Supplementary Table S10). Fifty-six intersecting genes were identified, which may be Pax3:Fkhr direct or indirect transcriptional targets.

Among those genes was *SKP2*, whose expression has been reported to be up-regulated by Pax3:Fkhr (25). The overexpression of *SKP2* gene in both mouse and human fusion-positive rhabdomyosarcoma was confirmed by qRT-PCR (Supplementary Fig. S3C). To determine whether *SKP2* transcription is regulated by Pax3:Fkhr, NIH3T3 cells were infected with a retrovirus carrying Pax3:Fkhr and then treated with cycloheximide for up to 8 hours (Fig. 5A). Treatment with cycloheximide did not affect *SKP2* levels during this time course, suggesting that *SKP2* transcription may be directly regulated by Pax3:Fkhr. To further study whether *SKP2* is a direct transcriptional target of Pax3:Fkhr, a reporter assay was performed using the *SKP2* promoter (Fig. 5B). Serially deleted genomic fragments from the *SKP2* promoter region (spanning the 3723bp fragment 5' upstream of *SKP2*) were tested for the response to Pax3:Fkhr overexpression in NIH3T3 cells. However, the *SKP2* promoter fragments did not show a transcriptional response to Pax3:Fkhr, although the *SKP2* promoter did respond to E2F1, a known direct transcription activator of *SKP2* gene (Fig. 5B; ref. 17).

Whereas the proximal 3.7kb *SKP2* promoter had no activity in response to Pax3:Fkhr, we speculated that Pax3:Fkhr may be up-regulating *SKP2* through another *cis*-element. In keeping with this hypothesis, Barber and colleagues reported from a chromatin immunoprecipitation screen that Pax3:Fkhr can bind to a 220-bp genomic fragment, which is 49 kb downstream (3') to the *SKP2* gene transcription initiation site (Supplementary Fig. S5; ref. 26). The distance, albeit long, is not unprecedented for genes involved in myogenic programming (27). This potential *cis*-element is conserved across species (Supplementary Fig. S5A). A reporter assay using this 220-bp genomic fragment showed increased luciferase activity when NIH3T3 cells or p53-deficient MEFs were cotransfected with Pax3:Fkhr, and like the *PDGFRA* reporter control (18), p53 may antagonize Pax3:Fkhr-mediated transcriptional activation of the *SKP2 cis*-element, depending upon the cellular context (antagonism was seen in NIH3T3 cells, but not in p53-deficient MEFs; Fig. 5C). Thus, this *cis*-element may be in at least one site by which Pax3:Fkhr regulates *SKP2*. A definite link between this Pax3:Fkhr responsive element and transcription of the *SKP2* gene will likely require future generation of new transgenic animals.

To determine the relevance of *SKP2* up-regulation by Pax3:Fkhr, we performed functional studies in human ARMS cells. *SKP2* has been reported to be involved in the cell cycle-dependent control of p27^{kip1} ubiquitination and, thus, cell cycle entry/tumor cell growth.

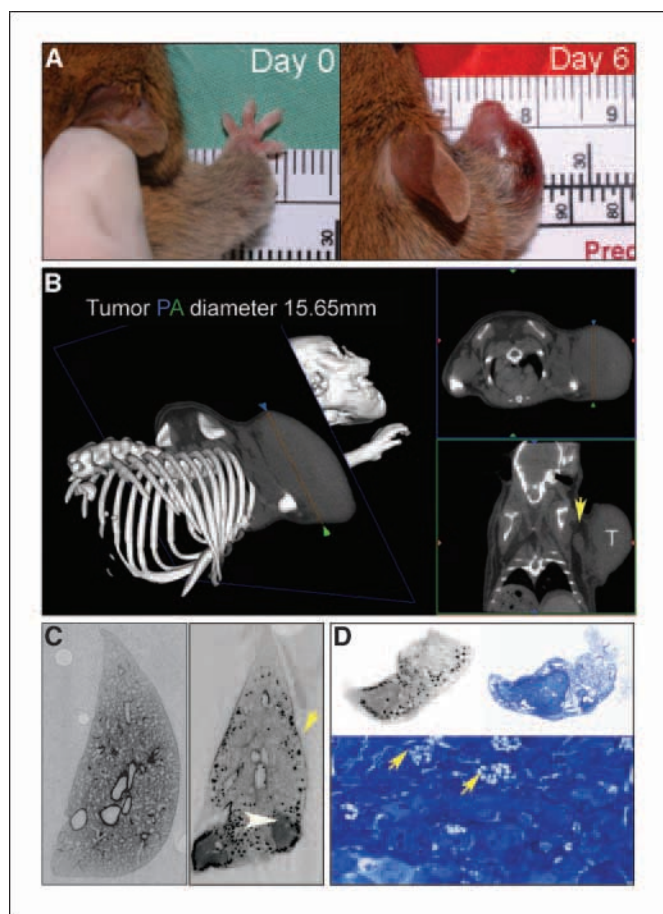


Figure 2. The conditional mouse model of ARMS reflects the aggressiveness of the human disease. *A*, limb tumor upon diagnosis (*left*) and at 6 d later (*right*). *B*, micro-CT scan of a right chest tumor (*T*). *Yellow arrow*, lymphatic metastasis; *PA*, posterior-anterior. *C*, pulmonary metastases can be quantified using micro-CT-based virtual histology. An 8- μ m resolution scan of normal lung (*left*) and lung with metastasis (*right*). *White arrows*, gross metastases ($0.8 \times 0.92 \times 0.74$ mm). *D*, comparison of scan (*top left*) and histology (*top right*). Histologic verification was performed after epoxy embedding. *Bottom*, higher magnification. *Yellow arrows* point to macrophages found in locations of black-appearing dots on the micro-CT scan. Macrophages are completely surrounded by tumor cells.

To determine whether *SKP2* repression can affect cell growth, the human ARMS cell line Rh30 was stably transfected with *SKP2*-specific short hairpin RNA (shRNA), as described previously (ref. 28; Fig. 5D). Increased protein level of p27kip1, as well as reduced expression of *SKP2*, was confirmed in *SKP2*-shRNA cells by Western blotting. Rh30 cells infected with *SKP2*-shRNA showed substantially reduced cell growth compared with control-shRNA cells. This effect was also confirmed in mouse ARMS cells, derived from a *Myf6^{ICNm/WT} Pax3^{P3Fm/P3Fm} p53^{F2-10/F2-10}* tumor (Supplementary Fig. S5B). Collectively, these data indicate that *SKP2* is a potential transcriptional target of Pax3:Fkhr via a 3' cis-element and that *SKP2* plays a major role in the cell proliferation of ARMS. More broadly, these results suggest that the mouse model of ARMS can serve to identify a *Pax3:Fkhr* molecular signature and Pax3:Fkhr target genes conserved across species.

The mouse model represents a system for evaluating kinase inhibitors for ARMS. This mouse model was previously used to validate a receptor tyrosine kinase, PDGFRA, as a direct transcriptional target of Pax3:Fkhr and therapeutic target (18). To identify other potential druggable targets in ARMS, we selected a subset of protein kinase genes that were up-regulated in both mouse and human ARMS tumors (Fig. 6A). Among 19 protein kinases up-regulated in mouse tumors, up-regulation of 16 kinases was conserved in human ARMS. From this set, kinase inhibitors are available against seven genes, including *VRK1*, *AURKB*, *PLK2*, *PLK4*, *CDK4*, *CHEK1*, and *TKI* (29–31). Overexpression of these kinases was confirmed by qRT-PCR in a larger set of mouse tumors (Fig. 6B). These results validate the future use of this mouse model as a preclinical tool for the study of therapeutic kinase inhibitor strategies in ARMS.

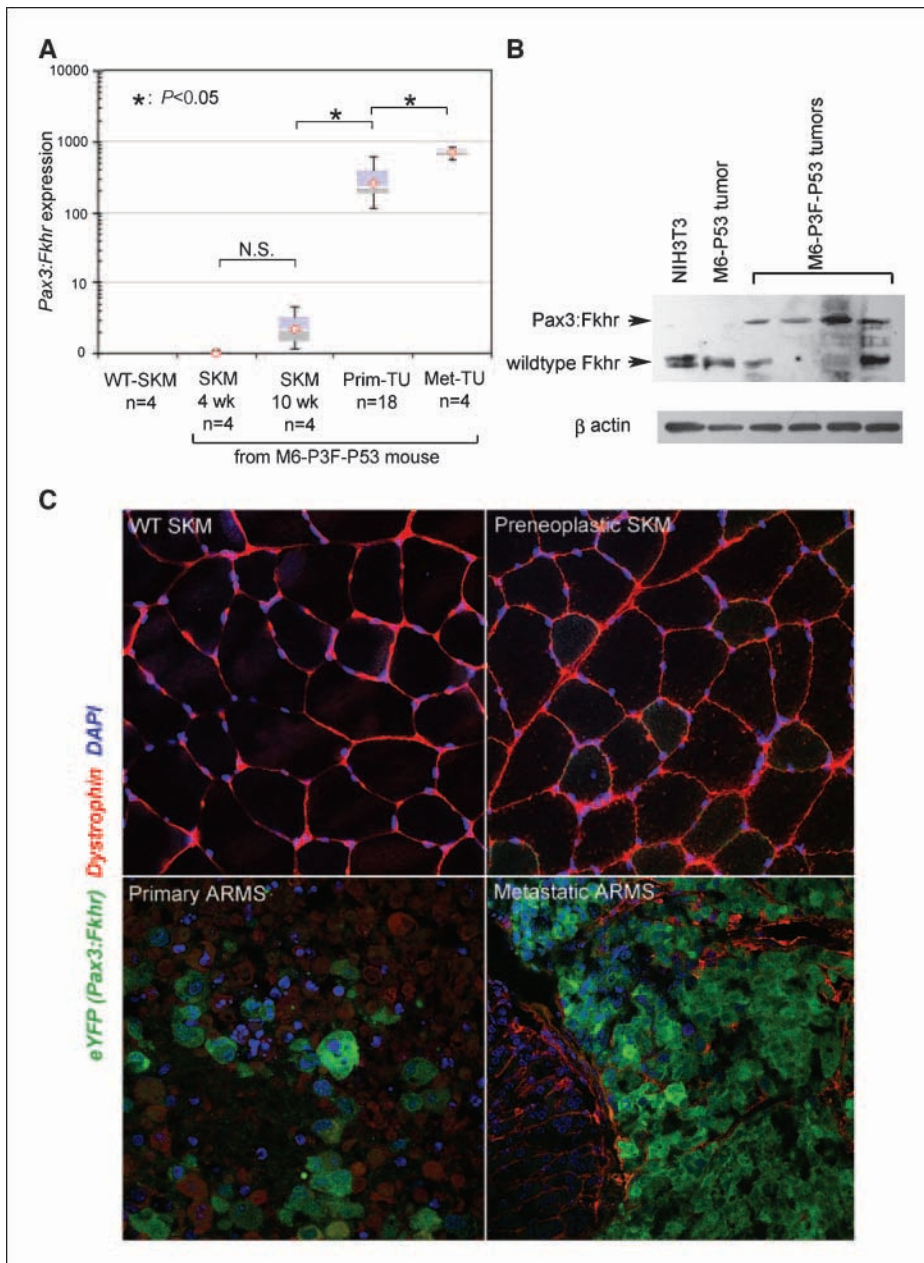


Figure 3. Stepwise increments in *Pax3:Fkhr* expression with disease progression. **A**, qPCR of *Pax3:Fkhr* expression in 4-wk-old WT skeletal muscle, 4-wk-old preneoplastic skeletal muscle, and tumors. *Pax3:Fkhr* was not detected in WT muscle (WT-SKM). Primary rhabdomyosarcoma tissue from *Myf6^{ICNm/WT} Pax3^{P3Fm/P3Fm} p53^{F2-10/F2-10}* (M6-P3F-p53 Prim-TU) mice expressed *Pax3:Fkhr* at a significantly higher level than the preneoplastic muscle of the same genotype. *Pax3:Fkhr* expression in metastatic tumor tissues (Met-TU) was significantly higher than primary tumors. *Pax3:Fkhr* expression was normalized relative to *Gapdh* expression. *C_t* values of *Pax3:Fkhr* PCR were 25 to 26 in mouse tumors. **B**, Pax3:Fkhr protein in mouse tumors using anti-Fkhr antibody. NIH3T3 cell lysate was used as a positive control for WT Fkhr. **C**, immunofluorescence of *Pax3:Fkhr* during disease progression (400×). A surrogate marker for *Pax3:Fkhr* expression was assayed using anti-GFP antibody (green) because both genes are expressed on the same mRNA by means of the *Pax3:Fkhr-ires-eYFP* allele. Red, dystrophin; blue, 4',6-diamidino-2-phenylindole (DAPI). Metastatic tumors taken from the liver contained a higher number of eYFP-expressing tumor cells than the primary tumor from the same animal.

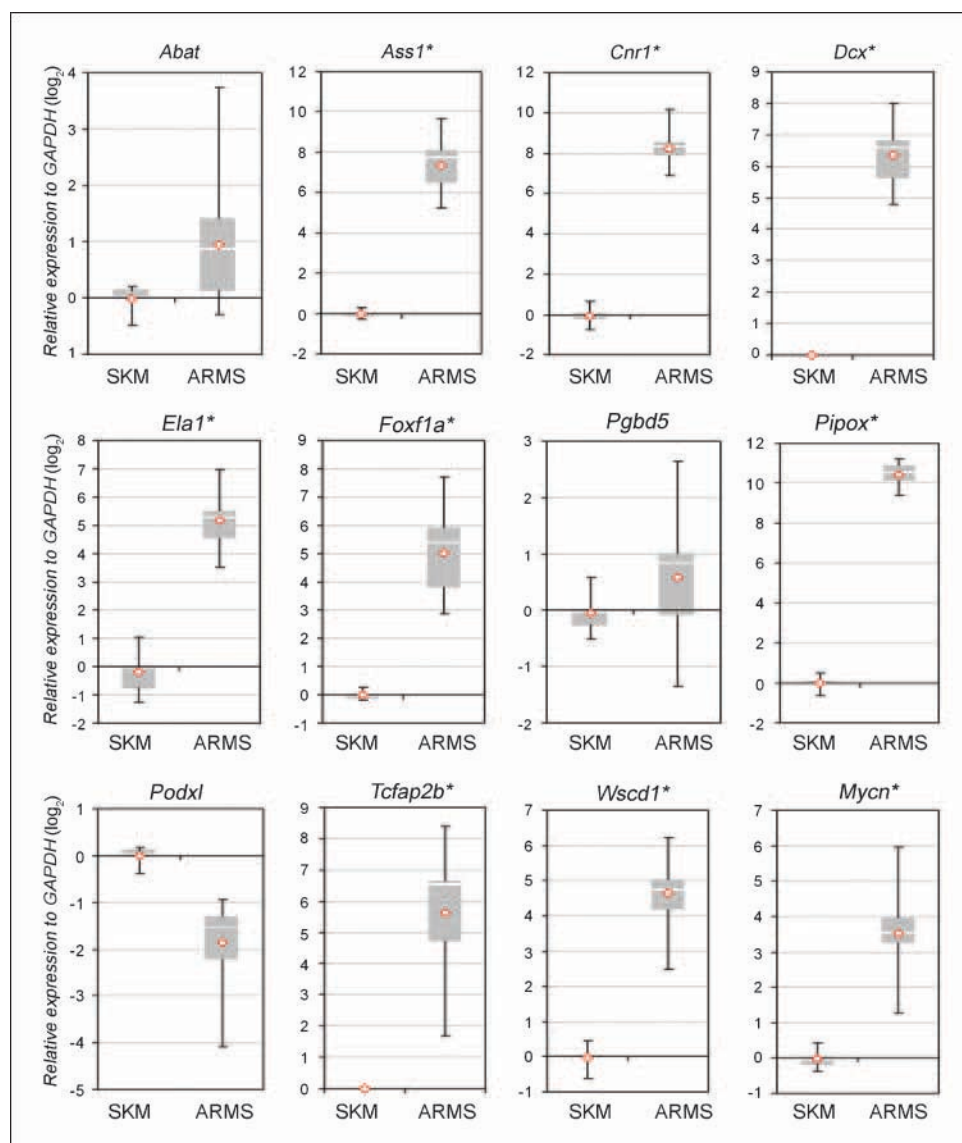


Figure 4. Expression of human ARMS-specific genes were studied by qRT-PCR in mouse ARMS tumors ($n = 10$) and skeletal muscles (SKM, $n = 6$). *, significant difference between mouse tumors and skeletal muscle ($P < 0.05$). Nine of 12 genes were significantly overexpressed in mouse tumors compared with skeletal muscle.

Discussion

In this paper, we present a cross-species validation of a genetically engineered mouse model of ARMS. The implicit advantage of using conditional genetic models for preclinical therapeutic testing are that tumors arise in an authentic microenvironment, i.e., skeletal muscle, and that the immune system is intact. The latter may be especially important for the promising cadre of monoclonal antibodies, for which antibody-dependent cellular cytotoxicity may require immunocompetence (32).

Our study shows that this ARMS model is advantageous for preclinical therapeutics for several reasons. We show that the *Pax3:Fkhr*, *p53* model has 100% penetrance by 150 days (young adulthood in a mouse) with a spectrum of disease sites that are comparable with human rhabdomyosarcoma. Histology and immunohistochemical markers also mimic the human disease, as reported here and previously (5, 7). Furthermore, the progression of disease in terms of primary tumor growth and extent of disease are as rapid as or more rapid than the human disease, making the

model useful for understanding the underlying disease mechanisms that allow unresectable or metastatic rhabdomyosarcoma to elude therapy.

We show at a cellular level that cooperative factors other than the *Pax3:Fkhr* fusion or *p53* inactivation are likely to be responsible for *Pax3:Fkhr* transcriptional regulation in preneoplastic muscle. However, once the primary tumor has formed, tumor cells that metastasize appear to be under selection for *Pax3:Fkhr* expression. Whereas targeting transcription factors, such as *Pax3:Fkhr*, is therapeutically challenging, one can hope that cooperative factors that facilitate high *Pax3:Fkhr* transcription might include cell surface receptors or proteins sensitive to small molecule inhibitors. The identification of these cooperative factors that modulate *Pax3:Fkhr* expression is the subject of ongoing studies.

To validate our model on a whole-genome basis, we performed a cross-species gene expression analysis. Gene set enrichment analysis confirmed that our model is most related to human ARMS among a variety of human sarcomas. We also performed metagene projection. This powerful method of cross-species,

cross-platform analysis (22) has been used recently to compare mouse and human pediatric cancer models among a variety of cancer subtypes. However, this method warrants some caution because results are dependent upon a training set with a large homogeneous collection of each tumor subtype. For rhabdomyosarcomas, which are relatively rare, sample size has been problematic in other studies (15). Nevertheless, we were able to show that, compared with other pediatric cancers, our mouse model is most similar to human rhabdomyosarcomas and

specifically human ARMS. We found, however, that despite using the best available microarray data set for rhabdomyosarcoma subtypes, metagene analysis could no better separate human *Pax:Fkhr*-positive ARMS from ERMS than the original report for this data set (9). This result may be due to a technical limitation of this approach and a small sample size or may suggest that ARMS and ERMS (as defined by histology) may be a continuous spectrum of disease. This later possibility, taken in a positive light, suggests that rhabdomyosarcomas might still be further subclassified on

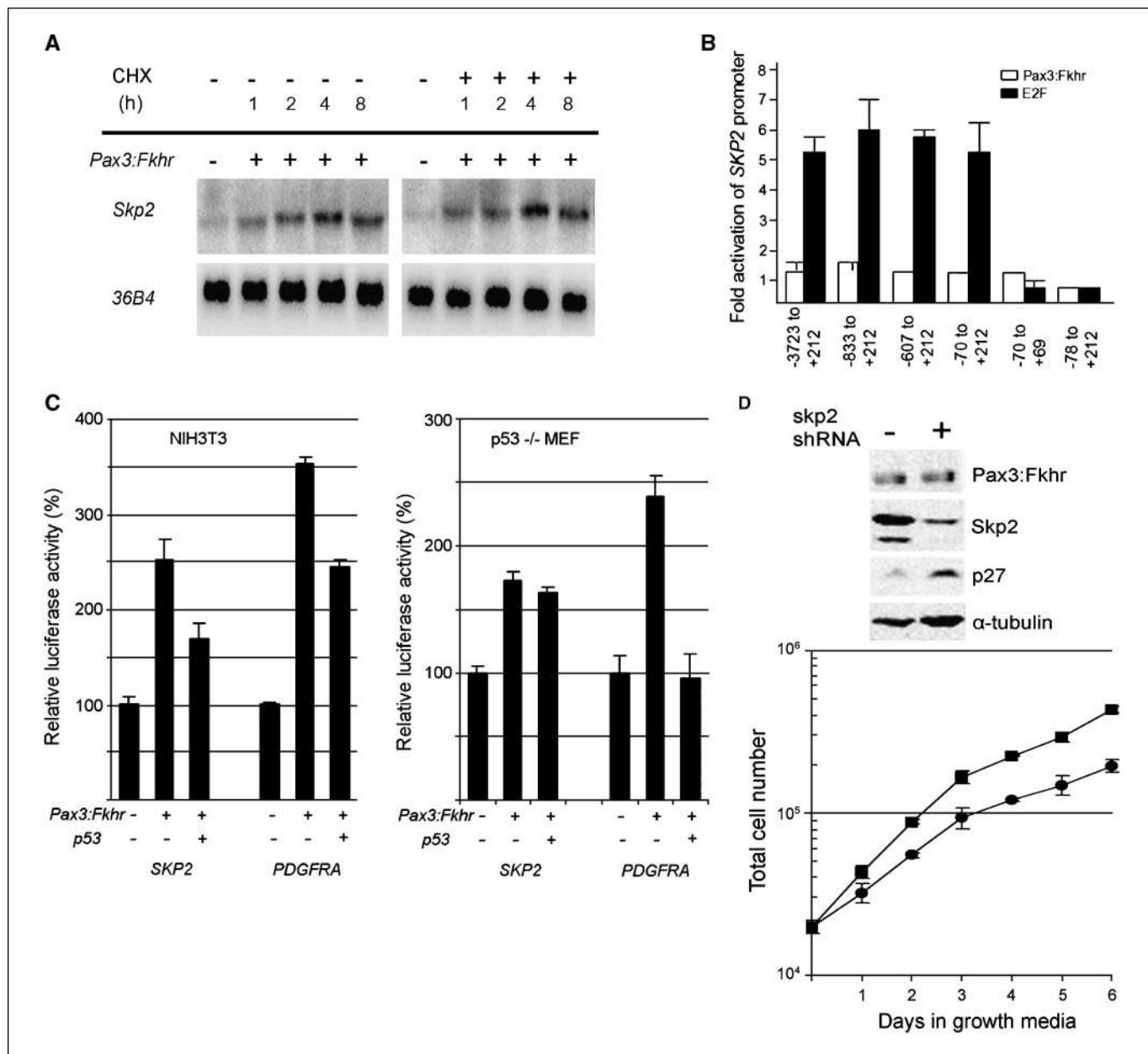


Figure 5. The mouse model phenocopies the human disease, allowing *Pax3:Fkhr* target identification. **A**, Northern blotting showed induction of *SKP2* expression by *Pax3:Fkhr* was maintained even after cycloheximide treatment. **B**, reporter assay showing a genomic fragment of 3,723 bp upstream to *SKP2* gene did not respond to *Pax3:Fkhr*. **C**, a putative *Pax3:Fkhr* binding site at 49 kb downstream (3') to *SKP2* showed response to *Pax3:Fkhr* in NIH3T3 cells and *p53*-deficient MEFs. *PDGFRA* promoter was used as a positive control. *, $P < 0.01$; N.S., no significant difference. **D**, *SKP2* down-regulation represses cell proliferation in human rhabdomyosarcoma cells. Rh30 was stably transfected with *SKP2*-specific or control shRNA vector. Western blot analysis confirmed reduced steady-state level of *SKP2* protein without affecting *PAX3-FKHR* protein level. Concomitant to reduced *SKP2* expression was an increase in *p27* protein. Rhabdomyosarcoma cells transfected with *SKP2*-specific shRNA showed substantially decreased cell growth compared with control nonspecific shRNA (analysis of covariance, $P < 0.001$). Population doubling time for *SKP2*-shRNA and nontargeting shRNA was 46.2 and 36.2 h, respectively.

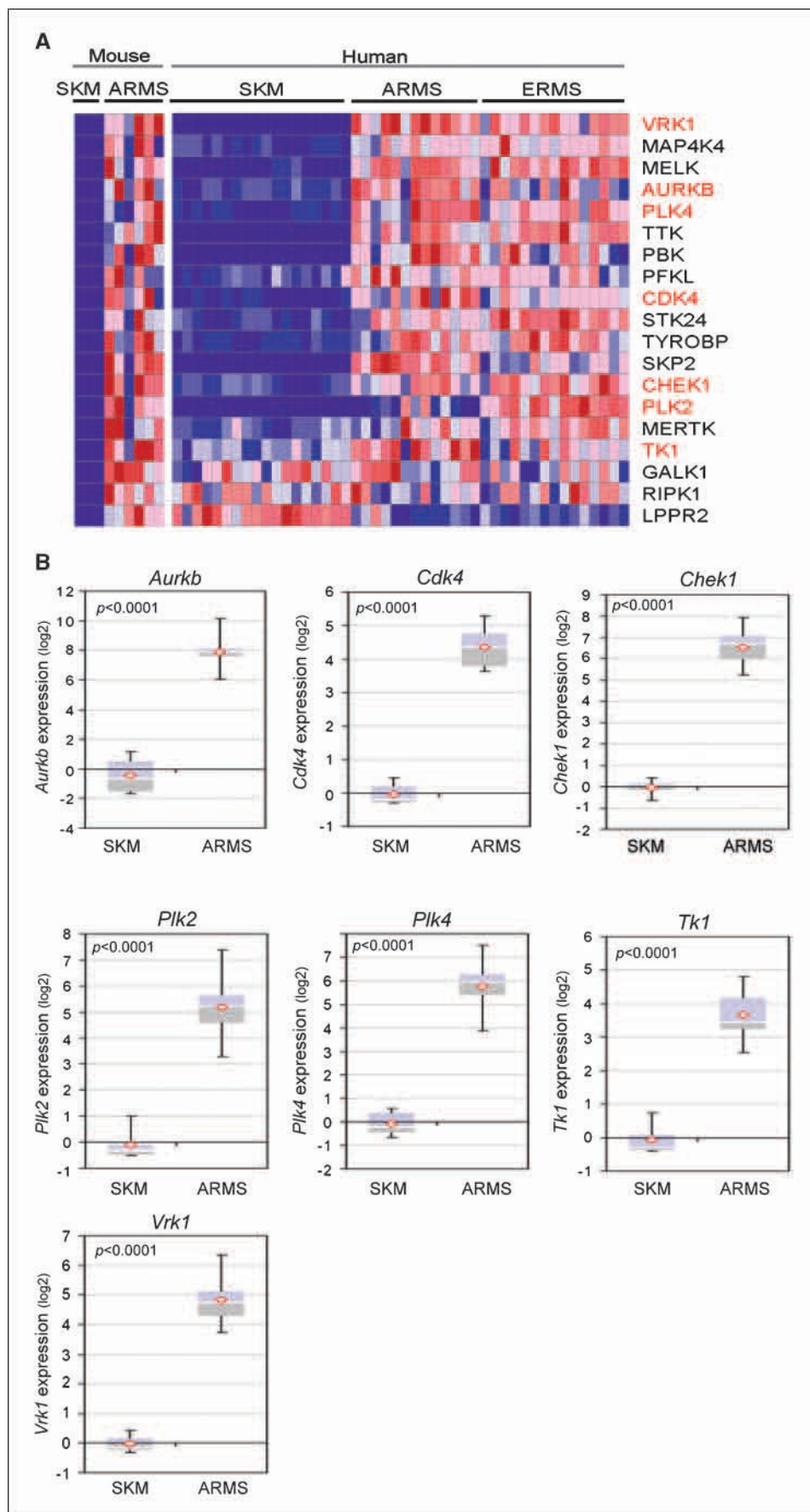


Figure 6. Cross-species identification of overexpressed protein kinases as potential therapeutic targets. *A*, expression pattern of 19 protein kinases overexpressed in mouse ARMS. Sixteen kinases were significantly up-regulated in human ARMS. Red-highlighted genes are potentially druggable targets. *B*, qRT-PCR confirming overexpression of the protein kinases for which kinase inhibitors are available.

molecular criteria beyond, or in addition to, *Pax:Fkhr* fusion status and histology.

We went on to identify 368 tumor-specific genes in common between mouse and human tumors that could neither be explained as being related to a normal muscle or degenerative muscle phenotype. Next, we used this genetic model to identify potential downstream targets of *Pax3:Fkhr*. Identifying *Pax3:Fkhr* targets has been the subject of numerous antecedent studies using many different valid approaches (i.e., transfection of rhabdomyosarcoma or nonrhabdomyosarcoma cells with *Pax3:Fkhr*, comparison between primary tumors, or combinations thereof; refs. 23, 26, 32–37). Our approach is meant only to be complementary. In the end, primary human tumor samples (*Pax3:Fkhr*-positive versus fusion-negative ARMS) are the definitive study set for such determinations, but getting large numbers of high-quality rapidly processed samples of these rare tumors has been a challenge for the field. Nevertheless, our cross-species approach identified 56 candidate target genes of *Pax3:Fkhr*, including *SKP2* (Fig. 5A, right). *SKP2* has been suggested to be a target gene of *Pax3:Fkhr*, but not *Pax3*, in fibroblasts (25). We have extended this result by validating *SKP2* as a *Pax3:Fkhr* target *in vivo*. *SKP2* is a component of the SCF (*SKP1-CUL1-F-box*) protein complex that mediates the ubiquitination and proteasomal degradation of cell cycle regulatory genes, including p27 (25, 38), thereby accelerating cell cycle progression. Ironically, *SKP2* also interacts with and promotes the ubiquitin-mediated degradation of *Fkhr* (*FoxO1A*; ref. 39). This *SKP2*-mediated degradation of *Fkhr* requires phosphorylation of *Fkhr* at Ser-256 (39), which is in fact retained by *Pax3:Fkhr* (40). Interestingly, *Fkhr* Ser-256 phosphorylation also reduces binding of *Fkhr* to DNA and causes nuclear exclusion of *Fkhr* when Thr-24 and Ser-319 are also phosphorylated (41). The extent to which the phosphorylation of this serine residue in *Pax3:Fkhr* can be enforced to take advantage of *SKP2* overexpression, SCF-mediated degradation, and *Pax3:Fkhr* nuclear exclusion is the topic of the ongoing investigation.

To identify new therapeutic targets, we examined the expression of potentially “druggable” kinases. The range of available kinase inhibitors is growing rapidly; therefore, we examined the cross-species rhabdomyosarcoma expression of kinases known to have an inhibitor available preclinically or clinically. We identified seven kinases, including an aurora kinase and two polo-like kinases.

¹⁵ Unpublished result.

References

- Arndt CA, Crist WM. Common musculoskeletal tumors of childhood and adolescence. *N Engl J Med* 1999;341:342–52.
- Stevens MC. Treatment for childhood rhabdomyosarcoma: the cost of cure. *Lancet Oncol* 2005;6:77–84.
- Davis RJ, D'Cruz CM, Lovell MA, Biegel JA, Barr FG. Fusion of PAX7 to FKHR by the variant t(1;13)(p36;q14) translocation in alveolar rhabdomyosarcoma. *Cancer Res* 1994;54:2869–72.
- Anderson J, Gordon T, McManus A, et al. Detection of the PAX3-FKHR fusion gene in paediatric rhabdomyosarcoma: a reproducible predictor of outcome? *Br J Cancer* 2001;85:831–5.
- Keller C, Arenkiel BR, Coffin CM, El-Bardeesy N, DePinho RA, Capecchi MR. Alveolar rhabdomyosarcomas in conditional *Pax3:Fkhr* mice: cooperativity of *Ink4a/ARF* and *Trp53* loss of function. *Genes Dev* 2004;18:2614–26.
- Keller C, Capecchi MR. New genetic tactics to model alveolar rhabdomyosarcoma in the mouse. *Cancer Res* 2005;65:7530–2.
- Keller C, Hansen MS, Coffin CM, Capecchi MR. *Pax3:Fkhr* interferes with embryonic *Pax3* and *Pax7* function: implications for alveolar rhabdomyosarcoma cell of origin. *Genes Dev* 2004;18:2608–13.
- Wachtel M, Dettling M, Koscielniak E, et al. Gene expression signatures identify rhabdomyosarcoma subtypes and detect a novel t(2;2)(q35;p23) translocation fusing PAX3 to NCOA1. *Cancer Res* 2004;64:5539–45.
- Lae M, Ahn EH, Mercado GE, et al. Global gene expression profiling of PAX-FKHR fusion-positive alveolar and PAX-FKHR fusion-negative embryonal rhabdomyosarcomas. *J Pathol* 2007;212:143–51.
- Kang PB, Kho AT, Sanoudou D, et al. Variations in gene expression among different types of human skeletal muscle. *Muscle Nerve* 2005;32:483–91.
- Bakay M, Zhao P, Chen J, Hoffman EP. A web-accessible complete transcriptome of normal human and DMD muscle. *Neuromuscul Disord* 2002;12 Suppl 1: S125–41.
- Wang HW, Trotter MW, Lagos D, et al. Kaposi sarcoma herpesvirus-induced cellular reprogramming contributes to the lymphatic endothelial gene expression in Kaposi sarcoma. *Nat Genet* 2004;36:687–93.
- Henderson SR, Guiliano D, Presneau N, et al. A molecular map of mesenchymal tumors. *Genome Biol* 2005;6:R76.
- Neale G, Su X, Morton CL, et al. Molecular characterization of the pediatric preclinical testing panel. *Clin Cancer Res* 2008;14:4572–83.
- Walkley CR, Qudsi R, Sankaran VG, et al. Conditional

For all of the strengths of this five allele genetically engineered model (more alleles if you include reporter genes for noninvasive imaging), significant infrastructure investments are required to maintain this disease model system. Because tumors can arise from deep sites, specialized small animal imaging technology is necessary (42) because traditional measurement with calipers at the skin surface nearly always underestimates the extent of disease. Luciferase has been surprisingly noninformative in our model system because tumors have a tendency to be centrally hypovascular and hypoxic (42), thereby unable to have access to the oxygen required by luciferase.¹⁵ The financial investment in maintaining mouse stock lines, husbandry, and genotyping is also nontrivial; therefore, alternative models, such as very successful rhabdomyosarcoma xenograft systems (43) and a recently reported ectopic allograft model (44), are warranted options to our transgenic model. In some instances, certain targets identified from human tumors are not expressed in the cell lines used for xenografts (18). In these cases, the genetically engineered model may not only be essential but also extremely productive. Our laboratory recently identified *PDGFRA* as a potential therapeutic target from the study of the ARMS preclinical model we report here (18). To follow this example and to make our model more practical for widespread use, we will be soon participating in the National Cancer Institute Pediatric Preclinical Testing Program (45, 46), with the intent of examining efficacy of novel targeted therapies. We will also be providing preclinical testing for outside investigators on a high-volume, low-cost basis. In this cooperative framework, the outlook for new therapies in ARMS may be significantly improved.

Disclosure of Potential Conflicts of Interest

C. Keller: Ownership interest and consultant/advisory board, Numira Biosciences. The other authors disclosed no potential conflicts of interest.

Acknowledgments

Received 9/24/08; revised 12/30/08; accepted 1/8/09.

Grant support: Bradley J. Breidinger Memorial research award from Sarcoma Foundation of America (C. Keller), NIH grant CA074907 (C. Wang), NIH grant CA64202 (F.G. Barr), Alex's Lemonade Stand Foundation grant (K. Nishijo, and Scott Carter), Foundation grant (C. Keller and K. Nishijo). C. Keller is a member of the Clinical Trial Research Center (P30CA54174).

The costs of publication of this article were defrayed in part by the payment of page charges. This article must therefore be hereby marked *advertisement* in accordance with 18 U.S.C. Section 1734 solely to indicate this fact.

We thank Dr. Peter Houghton for graciously providing Rh30 and Drs. Louis Kunkel and Peter B. Kang for the data sets and their kind review of this manuscript.

- mouse osteosarcoma, dependent on p53 loss and potentiated by loss of Rb, mimics the human disease. *Genes Dev* 2008;22:1662–76.
16. Mao J, Ligon KL, Rakhlin EY, et al. A novel somatic mouse model to survey tumorigenic potential applied to the Hedgehog pathway. *Cancer Res* 2006;66:10171–8.
 17. Zhang L, Wang C. F-box protein Skp2: a novel transcriptional target of E2F. *Oncogene* 2006;25:2615–27.
 18. Taniguchi E, Nishijo K, McCleish AT, et al. PDGFR-A is a therapeutic target in alveolar rhabdomyosarcoma. *Oncogene* 2008;27:6550–60.
 19. Relaix F, Montarras D, Zaffran S, et al. Pax3 and Pax7 have distinct and overlapping functions in adult muscle progenitor cells. *J Cell Biol* 2006;172:91–102.
 20. Subramanian A, Tamayo P, Mootha VK, et al. Gene set enrichment analysis: a knowledge-based approach for interpreting genome-wide expression profiles. *Proc Natl Acad Sci U S A* 2005;102:15545–50.
 21. Langenau DM, Keefe MD, Storer NY, et al. Effects of RAS on the genesis of embryonal rhabdomyosarcoma. *Genes Dev* 2007;21:1382–95.
 22. Tamayo P, Scanfeld D, Ebert BL, Gillette MA, Roberts CW, Mesirov JP. Metagene projection for cross-platform, cross-species characterization of global transcriptional states. *Proc Natl Acad Sci U S A* 2007;104:5959–64.
 23. Davicioni E, Finckenstein FG, Shahbazian V, Buckley JD, Triche TJ, Anderson MJ. Identification of a PAX-FKHR gene expression signature that defines molecular classes and determines the prognosis of alveolar rhabdomyosarcomas. *Cancer Res* 2006;66:6936–46.
 24. Galindo RL, Allport JA, Olson EN. A *Drosophila* model of the rhabdomyosarcoma initiator PAX7-FKHR. *Proc Natl Acad Sci U S A* 2006;103:13439–44.
 25. Zhang L, Wang C. PAX3-FKHR transformation increases 26 S proteasome-dependent degradation of p27Kip1, a potential role for elevated Skp2 expression. *J Biol Chem* 2003;278:27–36.
 26. Barber TD, Barber MC, Tomescu O, Barr FG, Ruben S, Friedman TB. Identification of target genes regulated by PAX3 and PAX3-FKHR in embryogenesis and alveolar rhabdomyosarcoma. *Genomics* 2002;79:278–84.
 27. Buchberger A, Freitag D, Arnold HH. A homeo-paired domain-binding motif directs Myf5 expression in progenitor cells of limb muscle. *Development* 2007;134:1171–80.
 28. Bondar T, Kalinina A, Khair L, et al. Cul4A and DDB1 associate with Skp2 to target p27Kip1 for proteolysis involving the COP9 signalosome. *Mol Cell Biol* 2006;26:2531–9.
 29. Valbuena A, Vega FM, Blanco S, Lazo PA. p53 downregulates its activating vaccinia-related kinase 1, forming a new autoregulatory loop. *Mol Cell Biol* 2006;26:4782–93.
 30. Johnson EF, Stewart KD, Woods KW, Giranda VL, Luo Y. Pharmacological and functional comparison of the polo-like kinase family: insight into inhibitor and substrate specificity. *Biochemistry* 2007;46:9551–63.
 31. Tyler RK, Shpiro N, Marquez R, Evers PA. VX-680 inhibits Aurora A and Aurora B kinase activity in human cells. *Cell Cycle* 2007;6:2846–54.
 32. Ebauer M, Wachtel M, Niggli FK, Schafer BW. Comparative expression profiling identifies an *in vivo* target gene signature with TFAP2B as a mediator of the survival function of PAX3/FKHR. *Oncogene* 2007;104:5959–64.
 33. Begum S, Emani N, Cheung A, Wilkins O, Der S, Hamel PA. Cell-type-specific regulation of distinct sets of gene targets by Pax3 and Pax3/FKHR. *Oncogene* 2005;24:1860–72.
 34. Tomescu O, Xia SJ, Strezlecki D, et al. Inducible short-term and stable long-term cell culture systems reveal that the PAX3-FKHR fusion oncoprotein regulates CXCR4, PAX3, and PAX7 expression. *Lab Invest* 2004;84:1060–70.
 35. Epstein JA, Song B, Lakkis M, Wang C. Tumor-specific PAX3-FKHR transcription factor, but not PAX3, activates the platelet-derived growth factor α receptor. *Mol Cell Biol* 1998;18:4118–30.
 36. De Pitta C, Tombolan L, Albiero G, et al. Gene expression profiling identifies potential relevant genes in alveolar rhabdomyosarcoma pathogenesis and discriminates PAX3-FKHR positive and negative tumors. *Int J Cancer* 2006;118:2772–81.
 37. Khan J, Bittner ML, Saal LH, et al. cDNA microarrays detect activation of a myogenic transcription program by the PAX3-FKHR fusion oncogene. *Proc Natl Acad Sci U S A* 1999;96:13264–9.
 38. Frescas D, Pagano M. Deregulated proteolysis by the F-box proteins SKP2 and β -TrCP: tipping the scales of cancer. *Nat Rev* 2008;8:438–49.
 39. Huang H, Regan KM, Wang F, et al. Skp2 inhibits FOXO1 in tumor suppression through ubiquitin-mediated degradation. *Proc Natl Acad Sci U S A* 2005;102:1649–54.
 40. Benniselli JL, Fredericks WJ, Wilson RB, Rauscher FJ III, Barr FG. Wild type PAX3 protein and the PAX3-FKHR fusion protein of alveolar rhabdomyosarcoma contain potent, structurally distinct transcriptional activation domains. *Oncogene* 1995;11:119–30.
 41. Zhang X, Gan L, Pan H, et al. Phosphorylation of serine 256 suppresses transactivation by FKHR (FOXO1) by multiple mechanisms. Direct and indirect effects on nuclear/cytoplasmic shuttling and DNA binding. *J Biol Chem* 2002;277:45276–84.
 42. Kindlmann GL, Weinstein DM, Jones GM, Johnson CR, Capecchi MR, Keller C. Practical vessel imaging by computed tomography in live transgenic mouse models for human tumors. *Mol Imaging* 2005;4:417–24.
 43. Smith MA, Morton CL, Phelps DA, et al. Stage 1 testing and pharmacodynamic evaluation of the HSP90 inhibitor alvespimycin (17-DMAG, KOS-1022) by the pediatric preclinical testing program. *Pediatr Blood Cancer* 2008;51:34–41.
 44. Ren YX, Finckenstein FG, Abdueva DA, et al. Mouse mesenchymal stem cells expressing PAX-FKHR form alveolar rhabdomyosarcomas by cooperating with secondary mutations. *Cancer Res* 2008;68:6587–97.
 45. Houghton PJ, Morton CL, Tucker C, et al. The pediatric preclinical testing program: description of models and early testing results. *Pediatr Blood Cancer* 2007;49:928–40.
 46. Houghton PJ, Adamson PC, Blaney S, et al. Testing of new agents in childhood cancer preclinical models: meeting summary. *Clin Cancer Res* 2002;8:3646–57.